Tropical cyclones vertical structure from GNSS radio occultation: an archive covering the period 2001–2018

Elżbieta Lasota[1,2], Andrea K. Steiner[3,4], Gottfried Kirchengast[3,4], Riccardo Biondi[2]

[1]Institute of Geodesy and Geoinformatics, Wrocław University of Environmental and Life Sciences, Wrocław, 50356, Poland
[2]Dipartimento di Geoscienze, Università degli Studi di Padova, Padua, 35131, Italy
[3]Wegener Center for Climate and Global Change (WEGC), University of Graz, Graz, 8010, Austria
[4]Institute for Geophysics, Astrophysics, and Meteorology/Institute of Physics, University of Graz, Graz, 8010, Austria

Correspondence to: Riccardo Biondi (riccardo@biondiriccardo.it)

Abstract. Tropical Cyclones (TC) are natural destructive phenomena, which affect wide tropical and subtropical areas every year. Although the correct prediction of their tracks and intensity has improved over recent years, the knowledge about their structure and development is still insufficient. The Global Navigation Satellite System (GNSS) Radio Occultation (RO) technique can provide a better understanding of the TC because it enables to probe the atmospheric vertical structure with high accuracy, high vertical resolution, and global coverage in any weather conditions. In this work, we create an archive of co-located TC best tracks and RO profiles covering the period 2001-2018 and providing a complete view of the storms since the pre-cyclone status to the cyclone disappearance. We collected 1822 TC best tracks from the International Best Track Archive for Climate Stewardship and co-located them with 48313 RO profiles from seven satellite missions processed by Wegener Center for Climate and Global Change. We provide information about location and intensity of the TC, RO vertical profiles co-located within 3 hours and 500 km from the TC eye centre, and exact information about temporal and spatial distance between the TC centre and the RO mean tangent point. A statistical analysis shows how the archive well covers all the ocean basins and all the intensity categories. We finally demonstrate the application of this dataset to investigate the vertical structure for one TC example case. All the data files, separately for each TC, are publicly available in NetCDF format at https://doi.org/10.25364/WEGC/TC-RO1.0:2020.1 (Lasota et al., 2020).

1. Introduction

The Tropical Cyclones (TCs), known also as hurricanes in the North Atlantic Ocean and Northeast Pacific, typhoons in the Northwest Pacific and simply as cyclones in the South Pacific and Indian Ocean, are extreme weather events affecting the social lives of many people and the economy of entire countries. The understanding of the development of TCs have increased with the availability satellite measurements, but a decisive improvement was given in the last decade by the use of the Global Navigation Satellite System (GNSS) Radio Occultation (RO) technique allowing to profile the atmosphere with high vertical resolution and high accuracy (Anthes et al., 2008). The GNSS RO technique uses GNSS signals and Low Earth Orbit (LEO) receivers to profile the atmospheric refractivity, from which profiles of temperature, pressure and humidity (Kursinski et al., 1997) are retrieved in the moist atmosphere by using background information. The RO technique was developed for observing the Earth's atmosphere and climate (Anthes et al., 2008; Steiner et al., 2011). It became important for the analyses and forecast of extreme atmospheric events (Bonafoni et al., 2019) motivating the interest and the launch of several new public and private missions (Cirac-Claveras, 2019).

Cardinali (2009) showed the high impact of RO to improve weather forecast, especially in remote areas of the globe where no other instruments are available with high vertical resolution. Several studies demonstrated the impact of RO profiles to improve the TC track forecast with assimilation in Numerical Weather Prediction (NWP) models. Huang et al. (2005), for the first time, assimilated RO refractivity profiles to forecast the Typhoons Nari in 2001 and Nakri in 2002, which developed in the North Western Pacific Ocean. This study was followed by many others, focusing on cyclone events: Hurricane Ernesto 2006 (Liu et al., 2012), Typhoon Usagi 2007 (Kunii et al., 2012), Typhoons Jangmi 2008, Hagupit 2008 and Sinlaku 2008 (Hsiao et al.,

2012), super-cyclone Gonu 2007 (Anisetty et al., 2014), and tropical cyclone Phailin 2013 (Hima Bindu et al., 2016). Huang et al., (2010) were the first who analysed a complete TC season followed by Chen et al. (2015). In a recent study, Chen et al. (2020) assimilated RO data during the genesis of 10 TCs in the North Western Pacific Ocean in the period 2008-2010. The results confirmed the benefit of assimilation of RO refractivity improving the humidity estimation in the lower and the middle troposphere and thus the forecast of the TCs. However, RO data are now widely used to study the TCs structure and their impact on the surrounding atmosphere. Biondi et al. (2011a) investigated for the first time the vertical structure of typhoon Hondo 2008 and hurricane Bertha 2008 and found a clear signature of the TC cloud top height. Biondi et al., (2011b) demonstrated that the presence of a TC creates a large positive bending angle anomaly in the Upper Troposphere and Lower Stratosphere (UTLS) corresponding to the TC anvil cloud top. The validation of these results with radiosondes and the Cloud-Aerosol Lidar with Orthogonal Polarization (CALIOP) revealed that the bending angle can be used to detect the cloud top (Biondi et al., 2013) and the possible overshooting (Biondi et al., 2015). In a more recent study, Lasota et al. (2018) analysed the RO bending angle sensitivity to the presence of clouds in TCs showing a significant signature of clouds between 8 and 14 km of altitude.

With the advent of the RO, the scientific community was able to better understand the TC inner thermal structure and Water Vapour (WV) content at different layers. The TC track and intensity predictions, until 2006, were almost completely based on parameters such as surface temperature, cloud-top temperature, and surface winds at the outer radius (Brueske and Velden, 2003; Demuth et al., 2004; Dvorak, 1975; Kidder et al., 1978; Velden et al., 2006) from different remote sensing techniques such as infrared and microwave sounders and imagers (King et al., 1992), lidar (Poole et al., 2003), reflected light polarization (Knibbe et al., 2000) and oxygen A-band technique (Koelemeijer et al., 2002). Anthes et al. (2003) were the first, comparing RO soundings with radiosonde observations during the typhoon Toraji 2001. The results revealed that the RO temperature profiles were consistent within 1 K, whilst RO water vapour observations tended to be slightly drier than radiosonde measurements above the middle troposphere. A similar agreement between RO and dropsonde observations was presented by Anthes et al. (2011) for the typhoon Jangmi 2008. Anthes et al. (2008) demonstrated the importance of RO temperature and WV assimilation to forecast hurricane Ernesto in 2006 (Chen et al., 2014; Liu et al., 2012). Winterbottom and Xiao (2010) showed that the quality and the horizontal resolution of RO was high enough to study TCs, even before the Constellation Observing System for Meteorology, Ionosphere and Climate (COSMIC) 6-satellite mission was launched. However, thanks to the higher number of RO observations provided from COSMIC after 2006, it has been possible to get a better understanding of the TCs' thermal structure: a warm core in the troposphere (Zou and Tian, 2018), a cooling corresponding to the TC anvil top height (Biondi et al., 2013; Rivoire et al., 2016) and an increase of WV in the Lower Stratosphere (LS) above the outermost rainbands (Venkat Ratnam et al., 2016). Vergados et al. (2013) for the first time used more of 1500 RO temperature, water vapour and refractivity profiles to study the moist thermodynamic structure in the lower and the upper troposphere of 42 North Atlantic TCs in the period 2002-2010. The analysis showed that the RO observations are able to capture the dimension, eyewall and rainbands of the TCs at different stages. Especially, the gradual decrease and wavelike pattern of water vapour was observed with increasing distance from the TC centre. Furthermore, a drop of WV was noticed in the lower and upper troposphere when the TCs develop from a tropical depression to Category 1 intensity.

The tropopause layer is often affected by the presence of the TC and this is easily detectable by using the RO profiles. In particular, the high vertical resolution of RO profiles shows that the TC anvil top generates a double tropopause effect when it does not reach the tropopause level (Biondi et al., 2011b, 2013; Vergados et al., 2014) and the Tropical Tropopause Layer (TTL) thickness is reduced (Ravindra Babu et al., 2015; Venkat Ratnam et al., 2016). Deep convective towers, usually developed within the TC eyewall and rainbands, generate Gravity Waves (GW) transporting energy to the upper atmosphere. The high vertical resolution of RO can reveal the GW spectral characteristics (Chane Ming et al., 2014) associated with the presence of the TC and show how the intensification of the TC creates LS GW (Chane Ming et al., 2014; Rakshit et al., 2018). A comprehensive review on the use of RO observations to study TCs is given by Bonafoni et al. (2019).

GNSS RO data are processed by several processing centres (Danish Meteorological Institute – DMI, EUMETSAT, German Research Centre for Geosciences – GFZ, Jet Propulsion Laboratory – JPL, University Corporation for Atmospheric Research – UCAR, Wegener Center for Climate and Global Change – WEGC) each using a different processing scheme. Regular inter-comparison studies of RO products from different centres (Ho et al., 2009; Steiner et al., 2013) are performed to improve the data and to understand differences. Latest results showed that RO data from different processing centres are highly consistent in the UTLS and differences become larger above 25 km altitude (Steiner et al., 2020). In this work, we use the WEGC RO dataset.

The aim of this work is to provide a comprehensive archive covering the period 2001–2018 collecting all the available information about TCs together with co-located RO observations to be used as a background for future studies to improve the knowledge on TC structure and development, to better understand the pre-TC environment and to study the effect of TC in the UTLS structure. For each TC, the information about track and intensity are combined with all the RO vertical profiles available within 500 km and 3 hours. The manuscript describes the datasets used to create the archive, explains the methodology to co-locate the different datasets, shows the statistical analysis of data spatial distribution, highlights an example of possible use of the dataset, and finally remarks the uncertainties and capabilities.

2. Data and methods

2.1. RO profiles

We have used the GNSS RO products level 1b (L1b) and level 2 (L2) processed by the Wegener Center for Climate and Global Change (WEGC) through the Occultation Processing System (OPS) v5.6, which use University Corporation for Atmospheric Research (UCAR) version orbit and phase data (Schwärz et al., 2016; Angerer et al., 2017, see Table 1). Out of this archive, we have selected the data of the CHAllenging Minisatellite Payload (CHAMP) from 2001 to 2008 (Wickert et al., 2001), the Satélite de Aplicaciones Cientıficas (SAC-C) form 2001 to 2013 (Hajj et al., 2004), the Gravity Recovery And Climate Experiment A (GRACE-A) from 2007 to 2017 and GRACE-B from 2014 to 2017 (Beyerle et al., 2005), the Constellation Observing System for Meteorology, Ionosphere and Climate (COSMIC) from 2006 to 2018 (Anthes et al., 2008), the Meteorological Operational satellite (MetOp) from 2008 to 2018 (Luntama et al., 2008), and the Communications/Navigation Outage Forecasting System (C/NOFS) from 2010 to 2011 (de La Beaujardière, 2004). The WEGC RO OPSv5.6 product includes vertical profiles of various variables including specific humidity, temperature, refractivity and bending angle of the atmosphere with 100 meter vertical sampling from near the surface altitude up to 60 km height with global coverage.
In the regions where the water vapour is negligible (usually above 10 km of altitude), the refractivity profiles can be transformed in dry temperature and dry pressure profiles by using a reduced refractivity equation (Scherlling-Pirscher et al., 2011). In the lower troposphere, the abundant amount of water vapour makes the dry air assumption not valid and ancillary information from weather model are required to retrieve the physical atmospheric parameters. The details of the OPSv5.6 tropospheric retrieval scheme is described by Li et al. (2019) introducing the moist air retrieval algorithm, inter-comparing it with the UCAR/COSMIC and EUMETSAT Radio Occultation Meteorology Satellite Application Facility (ROM SAF) retrievals and showing that in the lower to middle troposphere the moisture information is predominantly coming from the RO data. These results are also confirmed by Rieckh et al. (2018), that inter-compared tropospheric humidity profiles from four retrievals (including OPSv5.6) with radiosondes.
Furthermore, we made use of global monthly mean multi-satellite climatologies processed by the WEGC (based on OPSv5.6 profiles in the period 2001-2017). The climatological profiles of bending angle, specific humidity and temperature are available with 2.5°×2.5° horizontal resolution.

2.2. TC tracks

In this work, we focused on the TCs that occurred in the period 2001–2018 overlapping with the RO data availability. The comprehensive information of TC best tracks data was downloaded from the International Best Track Archive for Climate Stewardship (IBTrACS) version 04 (Knapp et al., 2010, 2018). The IBTrACS collects and combines the best tracks data from each World Meteorological Organization (WMO) Regional Specialized Meteorological Centers (RSMC) and Tropical Cyclone Warning Centers (TCWC), but also from other meteorological agencies, who trace the TCs in the regions of the interest.
In this dataset, we store the wind speeds and central pressures obtained from the WMO responsibility agency for the particular ocean basin. The RSMC and the TCWC participate in the Tropical Cyclone Programme (World Meteorological Organization, 1980) and are officially required to forecast and report the information about TC position, movement, and intensity in the designated area of responsibility (Table 1).

The IBTrACS dataset is disseminated in different formats, CSV, netCDF or shapefile formats, for various subsets such as for separate ocean basins, time periods, or for all TCs in the record. The archive is based on post-seasonal reanalyses and comprises information about storm name, position, maximum sustained wind speed or minimum central pressure, mostly reported with 6-hour temporal resolution, and some additional parameters interpolated to 3-hour resolution. The RSMC and TCWC compute and average the maximum sustained wind speed in different periods and hence, cannot be directly compared. The US agencies use a 1-minute averaging period, the Indian RSMC uses a 3-minute averaging period, whilst the rest of RSMC and TCWC (Brisbane, La Reunion, Nadi, Tokyo, Wellington) use a common 10-minute averaging period. The IBTrACS does not perform any wind speed transformations and provides original data from each agency, leaving to the users the choice of method for interagency comparison. However, for the statistics and analyses presented in this paper, we follow the guidelines given by the WMO (Harper et al., 2010). Conversion factors between the 10 and 3-minute sustained wind speed into 1-minute wind speed are calculated using the equation E-2 from the World Meteorological Organization (WMO) "Guideline for converting between various wind averaging periods in tropical cyclone conditions" (Harper et al., 2010). Next, to unify reported wind speeds to 1-minute sustained wind speed, the original wind speeds are multiplied by the calculated conversion factors of 1.08 and 1.05 for 10-minute and 3-minute averaging periods, respectively. The resulting values are used as a reference to categorize the TC intensity according to the commonly used Saffir-Simpson hurricane scale (Simpson and Saffir, 1974), which identifies seven levels based on the wind speed (Table 2).

2.3. Co-location of TC and RO observations

Retrieving RO profiles demands the appropriate knowledge of geometry between the Low Earth Orbit (LEO) receiver and GNSS satellites, which results in the random distribution of profiles in the time and space. Furthermore, the retrieved tangent point trajectory is curved and diverges from the vertical line since the GNSS and LEO satellites move with different speeds on non-coplanar orbits (Foelsche et al., 2011). In this work, we use the latitudes and longitudes of mean tangent points provided in the WEGC RO products. We co-locate each TC best track position with RO profiles which occurred within 3-hour and 500 km from the TC eye centre. The temporal window has been chosen as half temporal resolution of the TC best track reports, while the space window is chosen as a commonly used average TC radius of influence (Barlow, 2011; Knaff et al., 2013), which also corresponds to the half maximum path covered by a TC in 6 hours. In fact, we have computed in our dataset a maximum, minimum and average distances covered in 6 hours by a TC as 969.2 km, 0 km and 110.4 km, respectively. Thus, a single RO profile could be co-located with more than one TC best track position. In this case, we classified it to each TC track position, which meets the spatial and time condition.
As an example, we report in Figure 1 the best track of the hurricane Rick 2009 which developed from 14 October 2009 to 21 October 2009 in the Eastern Pacific Ocean basin close to the Mexican shore. The dots represent the TC eye centre, the circle indicates the 500 km radius that we have chosen as reference, and the colours show the TC intensity (from TD in blue to Cat. 5 in red). The stars denote the position of the co-located RO mean tangent point, and it becomes clear how a RO profile can be associated to more than one TC stage.

2.4. Data structure of the archive

For each TC, at every single step reported by the IBTrACS, we store the information about the co-locations between the TC and the RO, the vertical structure of the TC provided by RO data and the background environment (Table 3~~Table 3~~). The TC is described by the basin of development, the name of responsible recording WMO agency, the distance of the TC from land, the date, time and coordinates at each 6-hour best track stage, the nature of the storm, the storm translation speed, the minimum central pressure and the maximum sustained wind speed provided by the responsible WMO agency and stored in 'wmo_pres' and 'wmo_wind' variables, respectively. The co-locations between TCs and ROs are detailed with date, time and coordinates of the RO, the temporal difference between the co-located RO profile and the TC best track time, and the spatial distance between the RO mean tangent point and the TC best track coordinates. The TC vertical structure is given by the vertical profile from the surface (0 km) to 60 km with 100 m sampling for specific humidity, pressure, temperature, refractivity and bending angle. As a reference, we also report the climatological profiles of specific humidity, temperature and bending angle in the same area in order to compute the vertical anomaly structure with respect to the climatology.

The NetCDF format has been developed to share the array-oriented scientific data, therefore, the structure of the TC-RO archive is arranged to fulfil the array structure requirement. All the data are stored in the up to 3D arrays with particular dimensions: N_{TC}, N_{maxRO}, and N_{alt}. N_{TC} refers to the total number of the TC best track positions, separately for each analysed TC, whilst N_{maxRO} corresponds to the maximum number of co-located RO profiles with a single TC track position. Since not every TC track position has as many RO co-locations as the value of N_{maxRO}, the variables such as latRO, lonRO, bending angle and others may contain empty values, which are filled with appropriate filling values. The dimension, N_{alt}, is the number of available RO vertical levels (refractivity, pressure, temperature or specific humidity) and by default is equal to 600.
All the details of data structure are reported in Annex1.

3. Results

We have collected 48313 co-locations between ROs and TCs from 1570 TCs, with at least one profile for 86% of the TCs occurring in the period 2001–2018 (1822 in total, Table 4). In the early period 2001–2006, the number of co-locations is limited to a few hundred because only CHAMP and SAC-C were in orbit. CHAMP started measuring in May 2001, and thus the year with the lowest number of co-colocations was 2001 (only 50). In 2006, the COSMIC 6-satellite constellation was launched and the number of co-locations increased to some thousands per year. The year with the largest number of co-locations was 2008 with 5482 coming from 99 TC tracks. The highest number of co-located profiles comes from the MetOp-A receiver (Table 5) due to the largest time range availability (11 years). The ocean basin with the highest number of co-locations (Table 6) is the Western Pacific, due to the larger number of TCs which are lasting for a longer period than the other ocean basins.
The co-locations are well distributed in all the ocean basins (Figure 2) with a small number very close to the TC eye centre (172 in total), 1793 co-locations very close or into the eyewall, and an increasing number moving away from the centre (Table 6). Since the TCs have different intensity and different characteristics according to the area where they develop (Biondi et al., 2015), we also report the statistics by ocean basin and by categories (Table 6 and Figure 3). The Western Pacific Ocean basin has the largest number (14310) of co-locations, well covering all the categories except Cat. 5. In the Eastern Pacific Ocean and North Atlantic Ocean basins, we found the largest number of co-locations for the highest intensity Cat. 5 (14).
Demonstrating the use of the provided archive for an exemplary case study, we report in Figure 4 the case of typhoon Hondo in 2008, which developed in the South Indian ocean and reached the maximum intensity of Cat. 4. Hondo started as a tropical depression on 2 February 2008. Two days later it intensified to a TS and quickly reached TC intensity (reddish dots Figure 4a) on 5 February 2008. The status of a TC persisted for five days, then it weakened to a TD until the end of its life on 29 February 2008. Hondo is the TC for which we found the highest number of RO co-locations (Figure 4a, black stars) with a total of 212 profiles, just two into the TC eye, 10 are close to the eyewall and 200 distributed between 100 km and 500 km from the TC centre. Thirty-eight profiles are co-located with the TC status, 15 with TS and 159 with TD. The maximum number of profiles for a single stage was four, co-located with the TD on 12 February 2008. Figure 4b shows the temperature profile evolution with the time and altitude. The black profiles mostly indicate the TC stages and the yellow profiles indicate the TD final stages. Figure 4c represents the temporal and vertical behaviour for specific humidity. The RO data clearly reveal the temporal development of the storm's vertical structure. For the case of Hondo, we find that during the TC stages the mid tropospheric thermal structure is warmer (warm TC inner core) and the upper troposphere is colder. Figure 5 shows how to use the full dataset, including information of the TC best tracks, the anomaly profiles and climatology profiles from RO for analysing the vertical thermal structure and understanding the behaviour of the storm. First, we use the TC best-tracks to distinguish between the different storm stages (TD, TS and TC in Figure 5). Then, we evaluate the anomaly profiles of the different RO variables bending angle, temperature, and specific humidity, which have been computed by subtracting the reference monthly climatology profile in the respective area from the individual profile. The anomaly profiles represent signatures created by the presence of the storm. Figure 5a shows the averaged bending angle anomalies for the TD, TS and TC status of Hondo. In the lower troposphere, a large negative anomaly in bending angle (relative to the climatology) is present due to the increase of humidity (Figure 5c) while in the mid troposphere, the negative bending anomaly is due to the storm's warm core (Figure 5b).

In the upper troposphere, a positive anomaly in bending angle is caused by the cold cloud top. The TD moves less humidity than TS and TC (Figure 5c). The warm core and cold cloud top are more distinct for TS and TC than for TD (Figure 5b).

4. Data availability

All the data used to create this archive are publicly available. The WEGC GNSS RO record OPSv5.6 with high quality atmospheric profiles is available online (https://doi.org/10.25364/WEGC/OPS5.6:2019.1) and archived at the Earth Observation Data Centre (EODC) (ftp://galaxy.eodc.eu/unigraz/wegcenter/). Detailed information on the retrieval and on data quality is given by Angerer et al. (2017). The RO reference climatology was computed from OPSv5.6 profiles, which were averaged to a 2.5° x 2.5° latitude and longitude grid (each grid point containing profiles within a 300 km radius). The monthly mean climatology was computed for the period for August 2006 to September 2017. The TC best tracks were obtained from the NOAA IBTrACS webpage (https://www.ncdc.noaa.gov/ibtracs/) in CSV, netCDF or shapefile format for all available storms.

The created RO-TC dataset is available online at https://wegcwww.uni-graz.at/data-store/WEGC/TC-RO1.0:2020.1 (Lasota et al., 2020), it can be downloaded via file transfer protocol (ftp) or secure file transfer protocol (sftp) and the instructions for data download with different operating systems are provided at https://support.eodc.eu/kb/faq.php?id=38. The dataset consists of yearly folders, which refer to the year of the start of the storm. Each TC is saved in a separate file in NetCDF-4 format in corresponding yearly directory. Filenames are self-explanatory with a format string NAME_year_IBTrACSuniqueID.nc. For example, file MERANTI_2016_2016253N13144.nc includes all atmospheric RO profiles co-located with the TC Meranti of IBTrACS ID 2016253N13144, which occurred in 2016. The description of the variables included in each dataset file can be found in Table 3 and Annex 1.

5. Discussion and conclusions

In this work, we provide a comprehensive archive of TCs vertical structure for the period 2001–2018. Three main products are provided, co-located in time and space: global TC best tracks, RO profiles, and RO climatological profiles. The archive can be used for different purposes for analysing the vertical thermodynamic structure of cyclones and the pre-cyclone environment. The distance between the GNSS RO and TC best track is computed using as reference the RO mean tangent point coordinates which usually corresponds to an altitude of about 12.5 km above the mean sea level, with a vertical resolution of about 100 meters (Zeng et al., 2019) and a horizontal resolution of about 60 km to 300 km (Gorbunov et al., 2004; Kursinski et al., 1997). The uncertainty given by the RO location must be summed to the TC best track position uncertainty which mainly depends on the intensity of the storm and on the number and type of instruments used for monitoring (Landsea and Franklin, 2013). The TC best tracks are post-storm analyses relying on many different observations (ground based, aircraft, satellite, radiosondes). The more intense the storm the more accurate is the determination of the position. The more observations are available the lower is the uncertainty. As an example, Landsea and Franklin (2013) report a position uncertainty of about 30 miles for storms in the Atlantic Ocean observed just by satellite and a position uncertainty of about 8 miles for major hurricanes observed by satellite, aircraft and ground based instruments. In the worst case, the total co-location error between GNSS RO and TC best track could be up to 200 km in remote areas of the globe where just the satellite measurements are available and where storm intensities are low.

Part of this archive has already been used for studying the TC cloud top altitude (Biondi et al., 2013) and to provide a characterization of the TC thermal structure and to detect TC overshooting for different ocean basins (Biondi et al., 2015). This demonstrates that, despite the uncertainties reported above, this archive is well suited for deepening our knowledge on TCs. This is the first comprehensive archive collecting information of TC vertical structure, including profiles with a high vertical resolution from the surface to the TC cloud top and above, and providing high accuracy for all the main atmospheric parameters determining the development and the dynamics of the TCs.

This dataset allows gaining a better knowledge of the TC inner structure especially in remote areas where ground based sensors or radiosondes are not available and which are difficult to reach by aircraft. The independency of the ROs from the weather conditions provides a unique opportunity to profile extreme weather events without any risk and with global coverage.

The GNSS RO technique is well established and the RO acquisitions are increasing thanks to the successfully launched COSMIC 2 mission, which will contribute to a better understanding of TCs, provide the necessary information to forecast the TC tracks with high accuracy and enable studying the diurnal changes of temperature during the extreme events. We believe that this archive is useful to get a better understanding of the TC development and intensification, and to increase our knowledge on the impact of TCs on the atmospheric structure.

6. Author contribution

EL downloaded the data, developed the software and analysed the dataset. EL and RB designed the work and wrote the manuscript. RB supervised the project and acquired the funding. GK and AS provided the RO data, contributed to the manuscript text, and reviewed the manuscript.

7. Competing interests

The authors declare that there is no conflict of interest regarding the publication of this article.

8. Acknowledgments

The work is accomplished in the frame of the VESUVIO project funded by the Supporting Talent in ReSearch (STARS) grant at Università degli Studi di Padova, IT. We thank Florian Ladstädter (WEGC) for providing the RO reference climatologies. We thank Armin Leuprecht (WEGC) for his support and guidance on all technical aspects of the archive files.

References

Angerer, B., Ladstädter, F., Scherllin-Pirscher, B., Schwärz, M., Steiner, A. K., Foelsche, U. and Kirchengast, G.: Quality aspects of the Wegener Center multi-satellite GPS radio occultation record OPSv5.6, Atmospheric Measurement Techniques, 10(12), 4845–4863, doi:https://doi.org/10.5194/amt-10-4845-2017, 2017.

Anisetty, S. K. A. V. P. R., Huang, C.-Y. and Chen, S.-Y.: Impact of FORMOSAT-3/COSMIC radio occultation data on the prediction of super cyclone Gonu (2007): a case study, Nat Hazards, 70(2), 1209–1230, doi:10.1007/s11069-013-0870-0, 2014.

Anthes, R. A., Kuo, Y.-H., Rocken, C., and Schreiner, W.: Atmospheric sounding using GPS radio occultation, MAUSAM, 54(1),25–38, 2003

Anthes, R. A., Bernhardt, P. A., Chen, Y., Cucurull, L., Dymond, K. F., Ector, D., Healy, S. B., Ho, S.-P., Hunt, D. C., Kuo, Y.-H., Liu, H., Manning, K., McCormick, C., Meehan, T. K., Randel, W. J., Rocken, C., Schreiner, W. S., Sokolovskiy, S. V., Syndergaard, S., Thompson, D. C., Trenberth, K. E., Wee, T.-K., Yen, N. L. and Zeng, Z.: The COSMIC/FORMOSAT-3 Mission: Early Results, Bull. Amer. Meteor. Soc., 89(3), 313–334, doi:10.1175/BAMS-89-3-313, 2008.

Anthes, R. A.: Exploring Earth's atmosphere with radio occultation: contributions to weather, climate and space weather, Atmospheric Measurement Techniques, 4, 1077–1103, doi:10.5194/amt-4-1077-2011, 2011.

Barlow, M.: Influence of hurricane-related activity on North American extreme precipitation, Geophysical Research Letters, 38(4), doi:10.1029/2010GL046258, 2011.

Beyerle, G., Schmidt, T., Michalak, G., Heise, S., Wickert, J. and Reigber, C.: GPS radio occultation with GRACE: Atmospheric profiling utilizing the zero difference technique, Geophysical Research Letters, 32(13), doi:10.1029/2005GL023109, 2005.

Biondi, R., Neubert, T., Syndergaard, S. and Nielsen, J.: Measurements of the upper troposphere and lower stratosphere during tropical cyclones using the GPS radio occultation technique, Advances in Space Research, 47(2), 348–355, doi:10.1016/j.asr.2010.05.031, 2011a.

Biondi, R., Neubert, T., Syndergaard, S. and Nielsen, J. K.: Radio occultation bending angle anomalies during tropical cyclones, Atmospheric Measurement Techniques, 4(6), 1053–1060, doi:https://doi.org/10.5194/amt-4-1053-2011, 2011b.

Biondi, R., Ho, S.-P., Randel, W., Syndergaard, S. and Neubert, T.: Tropical cyclone cloud-top height and vertical temperature structure detection using GPS radio occultation measurements, Journal of Geophysical Research: Atmospheres, 118(11), 5247–5259, doi:10.1002/jgrd.50448, 2013.

Biondi, R., Steiner, A. K., Kirchengast, G. and Rieckh, T.: Characterization of thermal structure and conditions for overshooting of tropical and extratropical cyclones with GPS radio occultation, Atmospheric Chemistry and Physics, 15(9), 5181–5193, doi:https://doi.org/10.5194/acp-15-5181-2015, 2015.

Bonafoni, S., Biondi, R., Brenot, H. and Anthes, R.: Radio occultation and ground-based GNSS products for observing, understanding and predicting extreme events: A review, Atmospheric Research, 230, 104624, doi:10.1016/j.atmosres.2019.104624, 2019.

Brueske, K. F. and Velden, C. S.: Satellite-Based Tropical Cyclone Intensity Estimation Using the NOAA-KLM Series Advanced Microwave Sounding Unit (AMSU), Mon. Wea. Rev., 131(4), 687–697, doi:10.1175/1520-0493(2003)131<0687:SBTCIE>2.0.CO;2, 2003.

Cardinali, C.: Monitoring the observation impact on the short-range forecast, Quarterly Journal of the Royal Meteorological Society, 135(638), 239–250, doi:10.1002/qj.366, 2009.

Chane Ming, F., Ibrahim, C., Barthe, C., Jolivet, S., Keckhut, P., Liou, Y.-A. and Kuleshov, Y.: Observation and a numerical study of gravity waves during tropical cyclone Ivan (2008), Atmospheric Chemistry and Physics, 14(2), 641–658, doi:https://doi.org/10.5194/acp-14-641-2014, 2014.

Chen, S.-Y., Wee, T.-K., Kuo, Y.-H. and Bromwich, D. H.: An Impact Assessment of GPS Radio Occultation Data on Prediction of a Rapidly Developing Cyclone over the Southern Ocean, Mon. Wea. Rev., 142(11), 4187–4206, doi:10.1175/MWR-D-14-00024.1, 2014.

Chen, Y.-C., Hsieh, M.-E., Hsiao, L.-F., Kuo, Y.-H., Yang, M.-J., Huang, C.-Y. and Lee, C.-S.: Systematic evaluation of the impacts of GPSRO data on the prediction of typhoons over the northwestern Pacific in 2008–2010, Atmospheric Measurement Techniques, 8(6), 2531–2542, doi:https://doi.org/10.5194/amt-8-2531-2015, 2015.

Chen, S.-Y., Kuo, Y.-H. and Huang, C.-Y.: The Impact of GPS RO Data on the Prediction of Tropical Cyclogenesis Using a Nonlocal Observation Operator: An Initial Assessment, Mon. Wea. Rev., 148(7), 2701–2717, doi:10.1175/MWR-D-19-0286.1, 2020.

Cirac-Claveras, G.: Weather Satellites: Public, Private and Data Sharing. The Case of Radio Occultation Data, Space Policy, 47, 94–106, doi:10.1016/j.spacepol.2018.08.002, 2019.

Demuth, J. L., DeMaria, M., Knaff, J. A. and Vonder Haar, T. H.: Evaluation of Advanced Microwave Sounding Unit Tropical-Cyclone Intensity and Size Estimation Algorithms, J. Appl. Meteor., 43(2), 282–296, doi:10.1175/1520-0450(2004)043<0282:EOAMSU>2.0.CO;2, 2004.

Dvorak, V. F.: Tropical Cyclone Intensity Analysis and Forecasting from Satellite Imagery, Mon. Wea. Rev., 103(5), 420–430, doi:10.1175/1520-0493(1975)103<0420:TCIAAF>2.0.CO;2, 1975.

Foelsche, U., Syndergaard, S., Fritzer, J. and Kirchengast, G.: Errors in GNSS radio occultation data: relevance of the measurement geometry and obliquity of profiles, Atmos. Meas. Tech., 4(2), 189–199, doi:10.5194/amt-4-189-2011, 2011.

Gorbunov, M. E., Benzon, H.-H., Jensen, A. S., Lohmann, M. S. and Nielsen, A. S.: Comparative analysis of radio occultation processing approaches based on Fourier integral operators, Radio Science, 39(6), 1–11, doi:10.1029/2003RS002916, 2004.

Hajj, G. A., Ao, C. O., Iijima, B. A., Kuang, D., Kursinski, E. R., Mannucci, A. J., Meehan, T. K., Romans, L. J., Juarez, M. de la T. and Yunck, T. P.: CHAMP and SAC-C atmospheric occultation results and intercomparisons, Journal of Geophysical Research: Atmospheres, 109(D6), doi:10.1029/2003JD003909, 2004.

Harper, B. A., Kepert, J. D. and Ginger, J. D.: Guidelines for converting between various wind averaging periods in tropical cyclone conditions, World Meteorological Organization, Geneva, Switzerland. [online] Available from: https://www.wmo.int/pages/prog/www/tcp/documents/WMO_TD_1555_en.pdf, 2010.

Hima Bindu, H., Venkat Ratnam, M., Yesubabu, V., Narayana Rao, T., Kesarkar, A. and Naidu, C. V.: Characteristics of cyclone generated gravity waves observed using assimilated WRF model simulations over Bay of Bengal, Atmospheric Research, 180, 178–188, doi:10.1016/j.atmosres.2016.05.021, 2016.

Hsiao, L.-F., Chen, D.-S., Kuo, Y.-H., Guo, Y.-R., Yeh, T.-C., Hong, J.-S., Fong, C.-T. and Lee, C.-S.: Application of WRF 3DVAR to Operational Typhoon Prediction in Taiwan: Impact of Outer Loop and Partial Cycling Approaches, Wea. Forecasting, 27(5), 1249–1263, doi:10.1175/WAF-D-11-00131.1, 2012.

Huang, C.-Y., Kuo, Y.-H., Chen, S.-H. and Vandenberghe, F.: Improvements in Typhoon Forecasts with Assimilated GPS Occultation Refractivity, Wea. Forecasting, 20(6), 931–953, doi:10.1175/WAF874.1, 2005.

Huang, C.-Y., Kuo, Y.-H., Chen, S.-Y., Terng, C.-T., Chien, F.-C., Lin, P.-L., Kueh, M.-T., Chen, S.-H., Yang, M.-J., Wang, C.-J. and Prasad Rao, A. S. K. A. V.: Impact of GPS radio occultation data assimilation on regional weather predictions, GPS Solut, 14(1), 35, doi:10.1007/s10291-009-0144-1, 2010.

Kidder, S. Q., Gray, W. M. and Vonder Haar, T. H.: Estimating Tropical Cyclone Central Pressure and Outer Winds from Satellite Microwave Data, Mon. Wea. Rev., 106(10), 1458–1464, doi:10.1175/1520-0493(1978)106<1458:ETCCPA>2.0.CO;2, 1978.

King, M. D., Kaufman, Y. J., Menzel, W. P. and Tanre, D.: Remote sensing of cloud, aerosol, and water vapor properties from the moderate resolution imaging spectrometer (MODIS), IEEE trans. geosci. remote sens, 30(1), 2–27, 1992.

Knaff, J. A., Longmore, S. P. and Molenar, D. A.: An Objective Satellite-Based Tropical Cyclone Size Climatology, J. Climate, 27(1), 455–476, doi:10.1175/JCLI-D-13-00096.1, 2013.

Knapp, K. R., Kruk, M. C., Levinson, D. H., Diamond, H. J. and Neumann, C. J.: The International Best Track Archive for Climate Stewardship (IBTrACS), Bull. Amer. Meteor. Soc., 91(3), 363–376, doi:10.1175/2009BAMS2755.1, 2010.

Knapp, K. R., Diamond, H. J., Kossin, J. P., Kruk, M. C. and Schreck, C. J. I.: International Best Track Archive for Climate Stewardship (IBTrACS) Project, Version 4., [online] Available from: https://doi.org/10.25921/82ty-9e16 (Accessed 1 August 2019), 2018.

Knibbe, W. J. J., de Haan, J. F., Hovenier, J. W., Stam, D. M., Koelemeijer, R. B. A. and Stammes, P.: Deriving terrestrial cloud top pressure from photopolarimetry of reflected light, Journal of Quantitative Spectroscopy and Radiative Transfer, 64(2), 173–199, doi:10.1016/S0022-4073(98)00135-6, 2000.

Koelemeijer, R. B. A., Stammes, P., Hovenier, J. W. and Haan, J. F. de: Global distributions of effective cloud fraction and cloud top pressure derived from oxygen A band spectra measured by the Global Ozone Monitoring Experiment: Comparison to ISCCP data, Journal of Geophysical Research: Atmospheres, 107(D12), AAC 5-1-AAC 5-9, doi:10.1029/2001JD000840, 2002.

Kunii, M., Seko, H., Ueno, M., Shoji, Y. and Tsuda, T.: Impact of Assimilation of GPS Radio Occultation Refractivity on the Forecast of Typhoon Usagi in 2007, Journal of the Meteorological Society of Japan. Ser. II, 90(2), 255–273, doi:10.2151/jmsj.2012-207, 2012.

Kursinski, E. R., Hajj, G. A., Schofield, J. T., Linfield, R. P. and Hardy, K. R.: Observing Earth's atmosphere with radio occultation measurements using the Global Positioning System, Journal of Geophysical Research: Atmospheres, 102(D19), 23429–23465, doi:10.1029/97JD01569, 1997.

de La Beaujardière, O.: C/NOFS: a mission to forecast scintillations, Journal of Atmospheric and Solar-Terrestrial Physics, 66(17), 1573–1591, doi:10.1016/j.jastp.2004.07.030, 2004.

Landsea, C. W. and Franklin, J. L.: Atlantic Hurricane Database Uncertainty and Presentation of a New Database Format, Mon. Wea. Rev., 141(10), 3576–3592, doi:10.1175/MWR-D-12-00254.1, 2013.

Lasota, E., Rohm, W., Liu, C.-Y. and Hordyniec, P.: Cloud Detection from Radio Occultation Measurements in Tropical Cyclones, Atmosphere, 9(11), 418, doi:10.3390/atmos9110418, 2018.

Lasota, E. Steiner, A. K., Kirchengast, G. and Biondi, R.: A comprehensive archive of Tropical cyclones vertical structure covering the period 2001-2018, University of Graz, Austria, doi:10.25364/WEGC/TC-RO1.0:2020.1, 2020.

Li, Y., Kirchengast, G., Scherllin-Pirscher, B., Schwaerz, M., Nielsen, J. K., Ho, S.-P., and Yuan, Y. B.: A New Algorithm for the Retrieval of Atmospheric Profiles from GNSS Radio Occultation Data in Moist Air and Comparison to 1DVar Retrievals, Remote Sens., 11, 2729, doi:10.3390/rs11232729, 2019.

Liu, H., Anderson, J. and Kuo, Y.-H.: Improved Analyses and Forecasts of Hurricane Ernesto's Genesis Using Radio Occultation Data in an Ensemble Filter Assimilation System, Mon. Wea. Rev., 140(1), 151–166, doi:10.1175/MWR-D-11-00024.1, 2012.

Luntama, J.-P., Kirchengast, G., Borsche, M., Foelsche, U., Steiner, A., Healy, S., von Engeln, A., O'Clerigh, E. and Marquardt, C.: Prospects of the EPS GRAS Mission For Operational Atmospheric Applications, Bull. Amer. Meteor. Soc., 89(12), 1863–1876, doi:10.1175/2008BAMS2399.1, 2008.

Poole, L. R., Winker, D. M., Pelon, J. R. and McCormick, M. P.: CALIPSO: global aerosol and cloud observations from lidar and passive instruments, in Sensors, Systems, and Next-Generation Satellites VI, vol. 4881, pp. 419–226, International Society for Optics and Photonics. [online] Available from: https://www.spiedigitallibrary.org/conference-proceedings-of-spie/4881/0000/CALIPSO--global-aerosol-and-cloud-observations-from-lidar-and/10.1117/12.462519.short?SSO=1 (Accessed 7 April 2020), 2003.

Rakshit, G., Jana, S. and Maitra, A.: Gravity Wave Behavior in Lower Stratosphere During Tropical Cyclones Over the Bay of Bengal, Radio Science, 53(11), 1356–1367, doi:10.1029/2018RS006614, 2018.

Ravindra Babu, S., Venkat Ratnam, M., Basha, G., Krishnamurthy, B. V. and Venkateswararao, B.: Effect of tropical cyclones on the tropical tropopause parameters observed using COSMIC GPS RO data, Atmospheric Chemistry and Physics, 15(18), 10239–10249, doi:https://doi.org/10.5194/acp-15-10239-2015, 2015.

Rieckh, T., Anthes, R., Randel, W., Ho, S.-P, and U. Foelsche, U.: Evaluating tropospheric humidity from GPS radio occultation, radiosonde, and AIRS from high-resolution time series, Atmos. Meas. Tech., 11, 3091–3109, doi:10.5194/amt-11-3091-2018, 2018.

Rivoire, L., Birner, T. and Knaff, J. A.: Evolution of the upper-level thermal structure in tropical cyclones, Geophysical Research Letters, 43(19), 10,530-10,537, doi:10.1002/2016GL070622, 2016.

Scherllin-Pirscher, B., Kirchengast, G., Steiner, A. K., Kuo, Y.-H., and Foelsche, U.: Quantifying uncertainty in climatological fields from GPS radio occultation: an empirical-analytical error model, Atmos. Meas. Tech., 4, 2019–2034, doi:10.5194/amt-4-2019-2011, 2011.

Schwärz, M., Kirchengast, G., Scherllin-Pirscher, B., Schwarz, J., Ladstädter, F. and Angerer, B.: Multi-Mission Validation by Satellite Radio Occultation–Extension Project, Final report for ESA/ESRIN, (01), 2016.

Simpson, R. H. and Saffir, H.: The hurricane disaster potential scale, Weatherwise, 27(8), 169, 1974.

Steiner, A. K., Lackner, B. C., Ladstädter, F., Scherllin-Pirscher, B., Foelsche, U. and Kirchengast, G.: GPS radio occultation for climate monitoring and change detection, Radio Science, 46(06), 1–17, doi:10.1029/2010RS004614, 2011.

Steiner, A. K., Ladstädter, F., Ao, C. O., Gleisner, H., Ho, S.-P., Hunt, D., Schmidt, T., Foelsche, U., Kirchengast, G., Kuo, Y.-H., Lauritsen, K. B., Mannucci, A. J., Nielsen, J. K., Schreiner, W., Schwärz, M., Sokolovskiy, S., Syndergaard, S., and Wickert, J.: Consistency and structural uncertainty of multi-mission GPS radio occultation records, Atmos. Meas. Tech., 13, 2547–2575, https://doi.org/10.5194/amt-13-2547-2020, 2020.

Velden, C., Harper, B., Wells, F., Beven, J. L., Zehr, R., Olander, T., Mayfield, M., Guard, C. "CHIP," Lander, M., Edson, R., Avila, L., Burton, A., Turk, M., Kikuchi, A., Christian, A., Caroff, P. and McCrone, P.: The Dvorak Tropical Cyclone Intensity Estimation Technique: A Satellite-Based Method that Has Endured for over 30 Years, Bull. Amer. Meteor. Soc., 87(9), 1195–1210, doi:10.1175/BAMS-87-9-1195, 2006.

Venkat Ratnam, M., Ravindra Babu, S., Das, S. S., Basha, G., Krishnamurthy, B. V. and Venkateswararao, B.: Effect of tropical cyclones on the stratosphere–troposphere exchange observed using satellite observations over the north Indian Ocean, Atmospheric Chemistry and Physics, 16(13), 8581–8591, doi:https://doi.org/10.5194/acp-16-8581-2016, 2016.

Vergados, P., Mannucci, A. J. and Su, H.: A validation study for GPS radio occultation data with moist thermodynamic structure of tropical cyclones, Journal of Geophysical Research: Atmospheres, 118(16), 9401–9413, doi:10.1002/jgrd.50698, 2013.

Vergados, P., Luo, Z. J., Emanuel, K. and Mannucci, A. J.: Observational tests of hurricane intensity estimations using GPS radio occultations, Journal of Geophysical Research: Atmospheres, 119(4), 1936–1948, doi:10.1002/2013JD020934, 2014.

Wickert, J., Reigber, C., Beyerle, G., König, R., Marquardt, C., Schmidt, T., Grunwaldt, L., Galas, R., Meehan, T. K., Melbourne, W. G. and Hocke, K.: Atmosphere sounding by GPS radio occultation: First results from CHAMP, Geophysical Research Letters, 28(17), 3263–3266, doi:10.1029/2001GL013117, 2001.

Winterbottom, H. R. and Xiao, Q.: An Intercomparison of GPS RO Retrievals with Colocated Analysis and In Situ Observations within Tropical Cyclones, Advances in Meteorology, 2010, e715749, doi:https://doi.org/10.1155/2010/715749, 2010.

World Meteorological Organization: Tropical Cyclone Programme Available from: https://www.wmo.int/pages/prog/www/tcp/ (Accessed 17 May 2020), 1980.

Zeng, Z., Sokolovskiy, S., Schreiner, W. S. and Hunt, D.: Representation of Vertical Atmospheric Structures by Radio Occultation Observations in the Upper Troposphere and Lower Stratosphere: Comparison to High-Resolution Radiosonde Profiles, J. Atmos. Oceanic Technol., 36(4), 655–670, doi:10.1175/JTECH-D-18-0105.1, 2019.

Zou, X. and Tian, X.: Hurricane Warm-Core Retrievals from AMSU-A and Remapped ATMS Measurements with Rain Contamination Eliminated, Journal of Geophysical Research: Atmospheres, 123(19), 10,815-10,829, doi:10.1029/2018JD028934, 2018.

Table 1. The list of main agencies included in the IBTrACS dataset in the different ocean basins: North Atlantic (NA), Eastern North Pacific (EN), Western North Pacific (WP), North Indian (NI), South Indian (SI), Southern Pacific (SP), South Atlantic (SA)

Agency	Abbreviation	Ocean basin
National Hurricane Center (NHC) of National Oceanic and Atmospheric Administration	hurdat_atl	NA
(NOAA, USA) as RSMC Miami	hurdat_epa	EN
Japan Meteorological Agency as RSMC Tokyo	tokyo	WP
India Meteorological Department as RSMC New Delhi	newdelhi	NI
Météo-France as RSMC La Reunion	reunion	SI
Australian Bureau of Meteorology as TCWC Perth, Darwin, Brisbane	bom	SI, SP
Meteorological Service of New Zealand, Ltd as TCWC Wellington	wellington	SP
Fiji Meteorological Service as RSMC Nadi	nadi	SP
Automated Tropical Cyclone Forecasting System for U.S. Department of Defense and National Weather Service TCWC	atcf	SA, NA, EP

Table 2. TC intensity based on the Saffir-Simpson Hurricane Wind Scale.

Category	Tropical Depression (TD)	Tropical Storm (TS)	Category 1 (Cat.1)	Category 2 (Cat.2)	Category 3 (Cat. 3)	Category 4 (Cat. 4)	Category 5 (Cat. 5)
1-minute maximum sustained wind speed [m s^{-1}]	≤17	18-32	33-42	43- 49	50-58	58-70	>70

Table 3 Parameters stored in the dataset files for each TC separately. N_{TC} denotes the number of TC track positions, N_{alt} the number of altitude levels (600 by default), N_{maxRO} stands for the maximum number of RO profiles found for a single TC best track position.

Parameter (unit)	Dimension	Description
altitude (m)	N_{alt} ×1	Altitudes above geoid between 0 and 59.9 km with 100 m spacing.
latTC (degrees north)	N_{TC}×1	Latitude of current TC track position.
lonTC (degrees east)	N_{TC}×1	Longitude of current TC track position.
basin	N_{TC}×1	Flag values (1-7) indicating the ocean basin for the current storm position: 1=East Pacific, 2=North Atlantic, 3=North Indian, 4=South Atlantic, 5=South Indian, 6=South Pacific, 7=Western Pacific
dist2land (km)	N_{TC}×1	Distance between current TC position and land.
landfall (km)	N_{TC}×1	Minimum distance of TC to land over next3 hours (0 means landfall).
nature	N_{TC}×1	Flag values (1–6) indicating the nature of the current TC stage: 1=Not Reported, 2=Disturbance, 3=Tropical System, 4=Extratropical System, 5=Subtropical System, 6=MIXED (occurs when agencies reported inconsistent types Not Reported)
storm_dir (degrees)	N_{TC}×1	Storm translation direction.
storm_speed (m s^{-1})	N_{TC}×1	Storm translation speed
subbasin	N_{TC}×1	Flag values (1-9) indicating ocean sub-basin for the current storm position: 1=Arabian Sea., 2=Bay of Bengal, 3=Central Pacific, 4=Caribbean Sea, 5=Gulf of Mexico, 6=North Atlantic, 7=Eastern Australia, 8=Western Australia, 9=No subbasin for this position
wmo_agency	N_{TC}×1	Flag values (1-10) indicating name of responsible WMO agency: 1=Not provided, 2=atcf, 3=bom, 4=hurdat_atl, 5=hurdat_epa, 6=nadi, 7=newdelhi, 8=reunion, 9=Tokyo, 10=wellington
wmo_pres (Pa)	N_{TC}×1	Minimum central pressure from responsible WMO agency.
wmo_wind (m s^{-1})	N_{TC}×1	Maximum sustained wind speed from responsible WMO agency.
RO_datetime (seconds since 1970-01-01 00:00:0.0)	N_{TC}×N_{maxRO}	Datetime of RO profile.
RO_ID	N_{TC}×64×N_{maxRO}	ID of collocated RO profile.
latRO (degrees north)	N_{TC}×N_{maxRO}	Latitude of mean RO tangent point.
lonRO (degrees east)	N_{TC}×N_{maxRO}	Longitude of mean RO tangent point.
QC	N_{TC}×N_{maxRO}	RO overall retriebal quality control (0 and 1 stand for good and bad profiles)
datediff_RO_TC (seconds)	N_{TC}×N_{maxRO}	Time difference between collocated RO profile and TC track position.
dist_RO_TC (km)	N_{TC}×N_{maxRO}	Distance between positions of TC track and mean RO tangent point.
bending_angle (rad)	N_{alt} ×N_{TC}×N_{maxRO}	Ionosphere corrected non-optimized RO bending angle profile.

bending_angle_climatology (rad)	$N_{alt} \times N_{TC} \times N_{maxRO}$	Corresponding monthly climatological RO bending angle profile with 2.5°×2.5° spatial resolution.
pressure (Pa)	$N_{alt} \times N_{TC} \times N_{maxRO}$	RO air pressure profile.
refracitivity	$N_{alt} \times N_{TC} \times N_{maxRO}$	RO refractivity profile.
specific_humidity ($kg \cdot kg^{-1}$)	$N_{alt} \times N_{TC} \times N_{maxRO}$	RO specific humidity profile.
specific_humidity_climatology ($kg \cdot kg^{-1}$)	$N_{alt} \times N_{TC} \times N_{maxRO}$	Corresponding monthly climatological RO specific humidity profile with 2.5° spatial resolution.
temperature (K)	$N_{alt} \times N_{TC} \times N_{maxRO}$	RO air temperature profile.
temperature_climatology (K)	$N_{alt} \times N_{TC} \times N_{maxRO}$	Corresponding monthly climatological RO air temperature profile with 2.5°×2.5° spatial resolution.

Table 4 Number of collocated RO profiles with TC with regard to the acquisition year.

Year	Number of profiles	Number of TC	Number of TC with at least 1 colocated RO profile
2001	50	107	23
2002	222	100	56
2003	310	107	74
2004	335	105	73
2005	310	115	71
2006	1969	100	98
2007	4187	94	94
2008	5482	99	99
2009	5119	100	99
2010	3640	88	88
2011	3739	95	95
2012	3585	93	93
2013	4471	103	103
2014	3932	91	91
2015	4339	112	111
2016	2909	95	95
2017	2017	107	101
2018	1697	111	106
Total	48313	1822	1570

Table 5 Number of collocated RO with TC for different RO satellites.

Satellite	Number of profiles

CHAMP	1881
CNOFS	519
F3C-FM1	6644
F3C-FM2	3954
F3C-FM3	1693
F3C-FM4	4969
F3C-FM5	5499
F3C-FM6	4918
GRACE-A	1836
GRACE-B	562
METOP-A	9416
METOP-B	4704
SAC-C	1718

Table 6 Number of collocated RO with TC with regard to the TC intensity and the distance to the TC eye on different ocean basins.

Basin	Distance	Intensity								
	[km]	Total	TD	TS	Cat. 1	Cat. 2	Cat. 3	Cat. 4	Cat. 5	Not available
NA	0-30	31	2	3	5	1	1	0	1	18
	31-100	280	43	69	10	7	6	6	3	136
	101-200	1021	149	254	63	27	13	9	0	506
	201-300	1698	253	443	114	42	25	16	1	804
	301-400	2243	324	597	116	43	23	31	4	1105
	401-500	2926	467	750	190	43	38	34	5	1399
	Total	8199	1238	2116	498	163	106	96	14	3968
EP	0-30	31	6	7	0	1	0	0	1	16
	31-100	346	85	62	15	5	3	7	0	169
	101-200	1109	252	188	40	25	22	14	2	566
	201-300	1920	442	338	93	28	22	18	3	976
	301-400	2666	616	455	120	52	39	24	1	1359
	401-500	3407	743	611	170	82	39	29	7	1726
	Total	9479	2144	1661	438	193	125	92	14	4812
WP	0-30	52	8	10	1	1	0	2	0	30
	31-100	567	98	79	48	23	20	6	0	293
	101-200	1722	307	252	119	45	60	11	0	928
	201-300	2787	521	390	219	79	103	26	0	1449

	301-400	4043	714	620	284	112	155	41	0	2117
	401-500	5139	863	773	390	159	157	45	0	2752
	Total	14310	2511	2124	1061	419	495	131	0	7569
NI	0-30	7	1	1	0	0	0	0	0	5
	31-100	88	27	15	8	2	0	2	0	34
	101-200	282	98	51	9	6	1	5	0	112
	201-300	486	184	72	10	8	5	5	0	202
	301-400	590	241	103	7	8	9	4	0	218
	401-500	823	294	118	27	10	20	7	0	347
	Total	2276	845	360	61	34	35	23	0	918
SA	0-30	0	0	0	0	0	0	0	0	0
	31-100	1	0	0	0	0	0	0	0	1
	101-200	16	7	1	0	0	0	0	0	8
	201-300	17	6	4	0	0	0	0	0	7
	301-400	27	9	3	0	0	0	0	0	15
	401-500	27	11	3	0	0	0	0	0	13
	Total	88	33	11	0	0	0	0	0	44
SP	0-30	13	2	2	1	1	1	0	0	6
	31-100	175	26	38	9	3	2	0	0	97
	101-200	538	81	101	27	7	13	1	2	306
	201-300	860	150	152	44	18	14	3	0	479
	301-400	1212	198	209	54	38	31	7	3	672
	401-500	1634	283	252	78	31	52	19	1	918
	Total	4432	740	754	213	98	113	30	6	2478
SI	0-30	38	12	5	2	0	0	0	0	19
	31-100	336	79	53	13	5	9	3	0	174
	101-200	1171	277	196	42	19	18	19	0	600
	201-300	1929	458	321	64	32	40	15	0	999
	301-400	2759	697	447	91	31	37	21	0	1435
	401-500	3296	840	541	98	53	39	24	1	1700
	Total	9529	2363	1563	310	140	143	82	1	4927
Total	0-30	172	31	28	9	4	2	2	2	94
	31-100	1793	358	316	103	45	40	24	3	904
	101-200	5859	1171	1043	300	129	127	59	4	3026
	201-300	9697	2014	1720	544	207	209	83	4	4916
	301-400	13540	2799	2434	672	284	294	128	8	6921
	401-500	17252	3501	3048	953	378	345	158	14	8855

	Total	48313	9874	8589	2581	1047	1017	454	35	24716

475

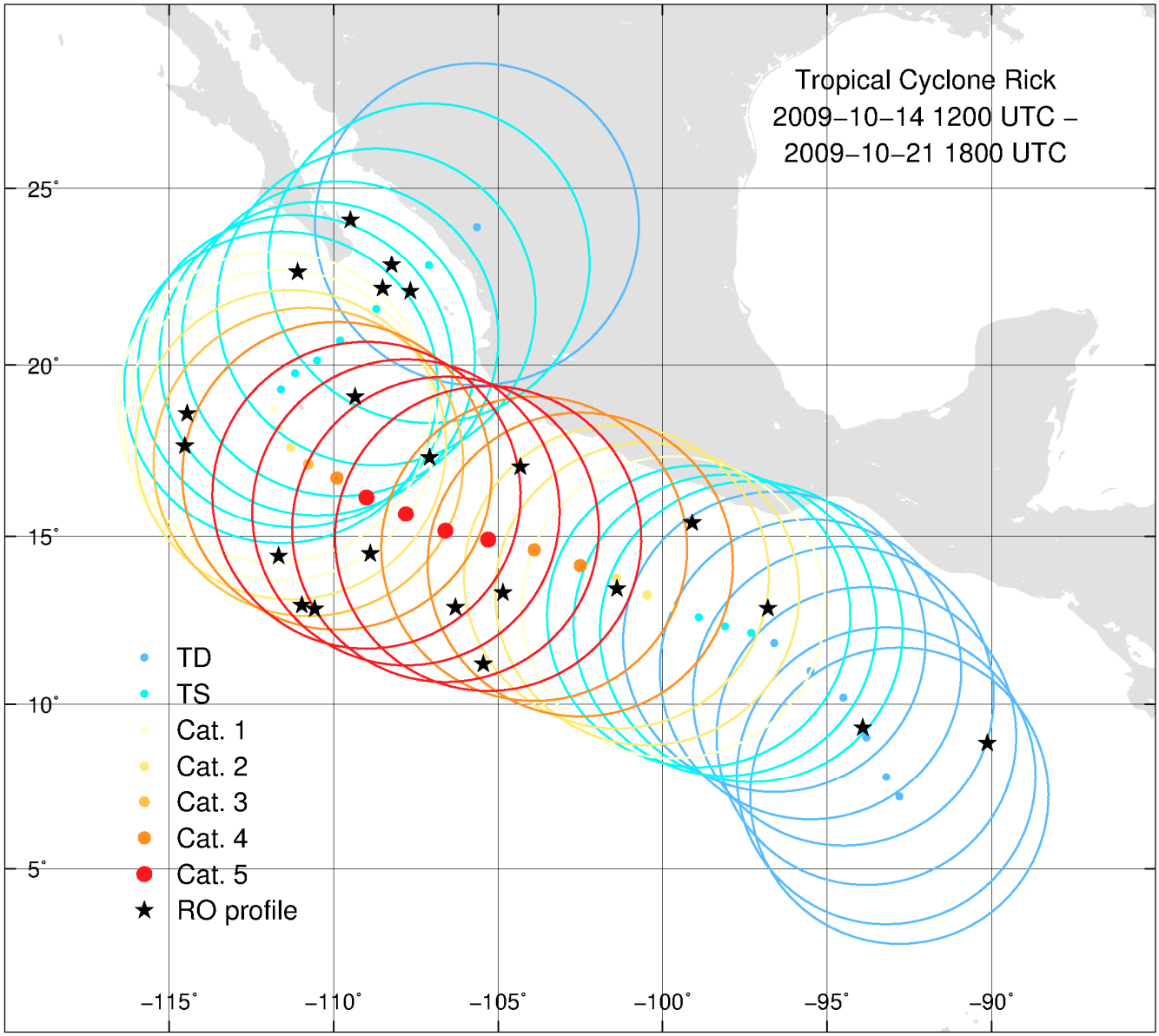

Figure 1 An example of co-location of TC with RO profiles (black stars) based on hurricane Rick developed between 14 and 21 October 2009. Dots present the TC eye position, whilst circles mark the 500 km co-location criterium. Colours indicate the intensity of TC.

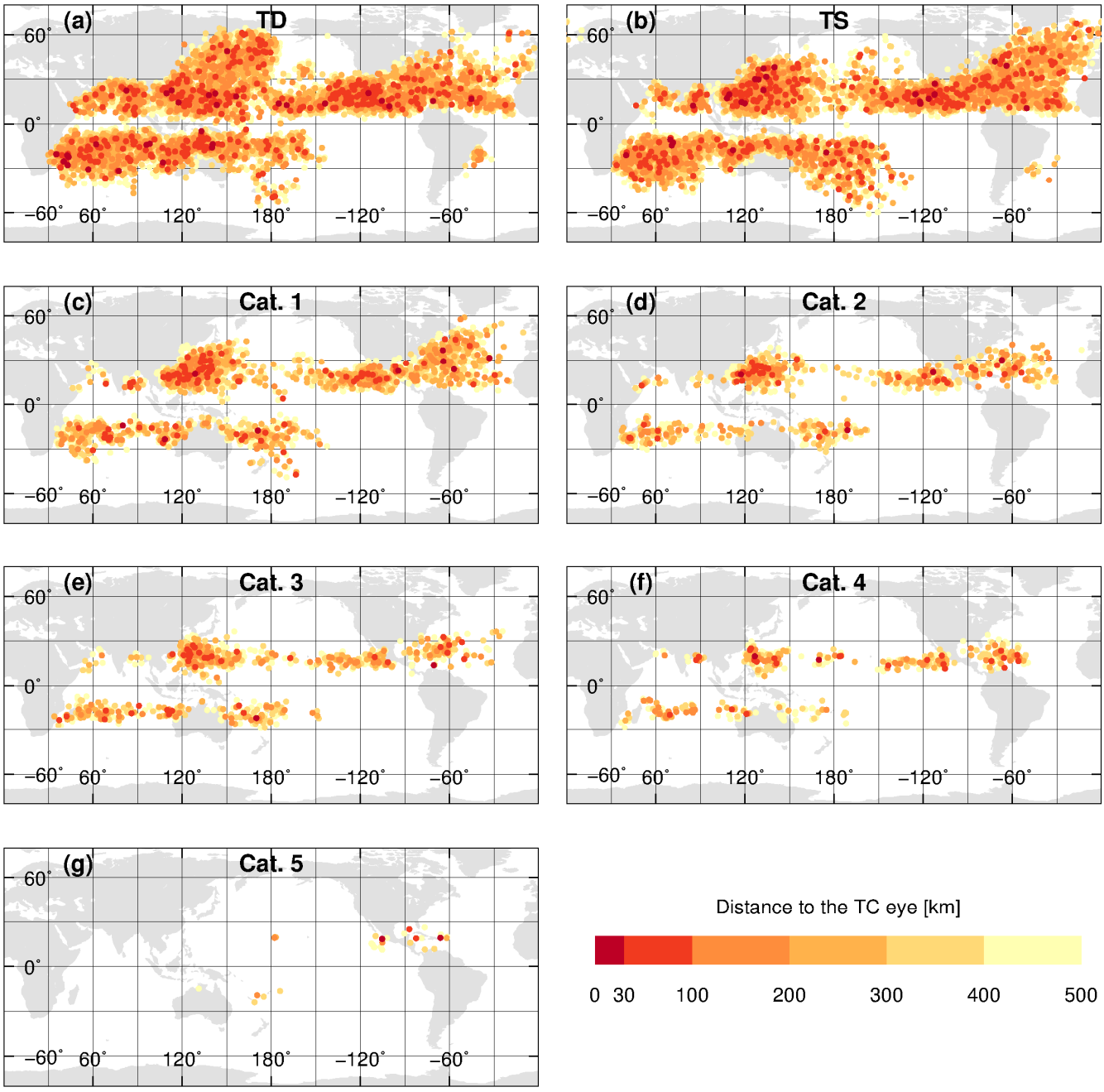

480

Figure 2 Map with distribution of RO profiles collocated with: (a) Tropical Depressions, (b) Tropical Storms, (c) TCs category 1, (d) TCs category 2, (e) TCs category 3, (f) TCs category 4, (g) TCs category 5. Colours denote the distances between RO profile and the nearest TC eye.

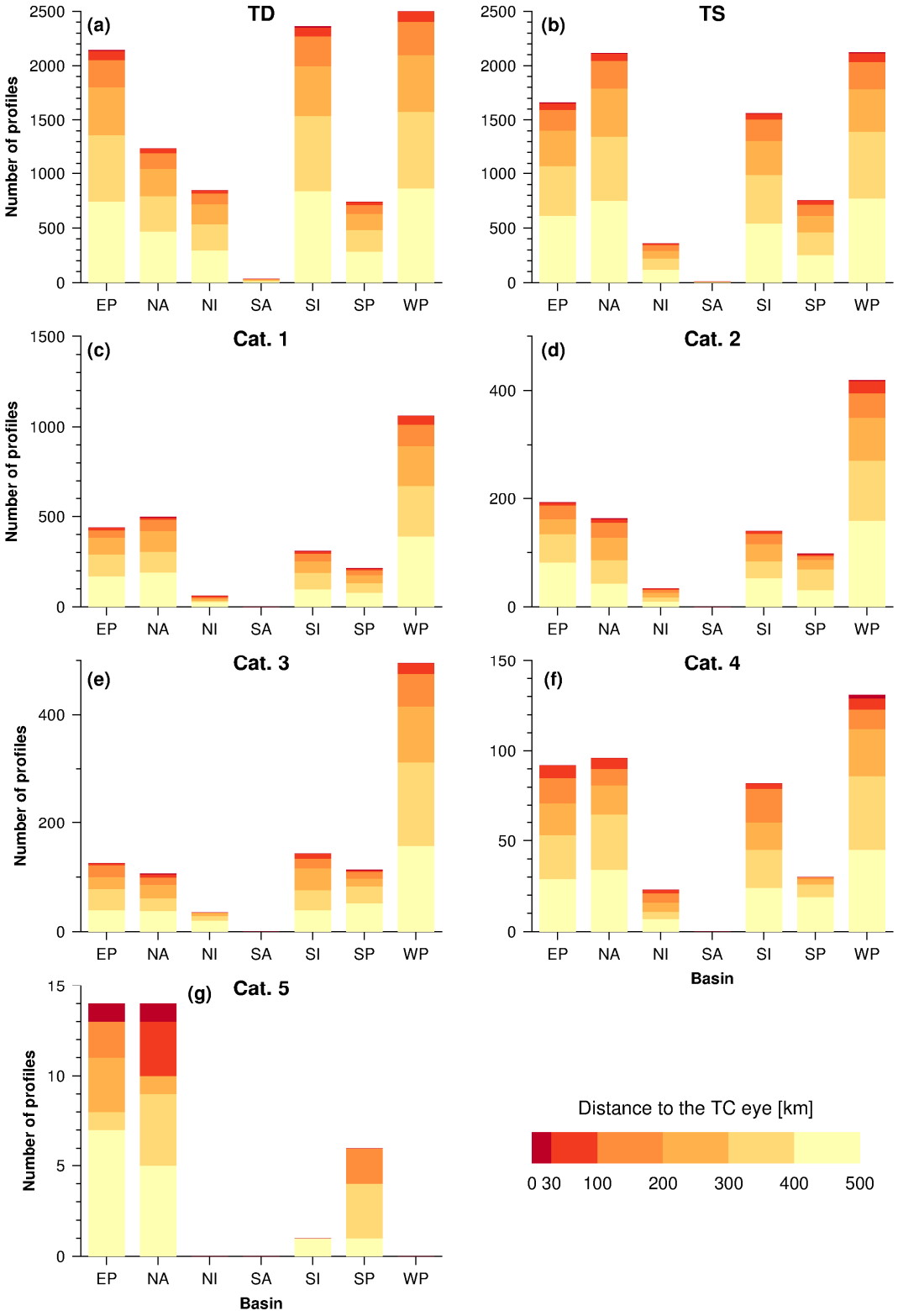
(a)
TD
(b)
TS
(c)
Cat. 1
(d)
Cat. 2
(e)
Cat. 3
(f)
Cat. 4
(g)
Cat. 5
Number of profiles
Basin
EP
NA
NI
SA
SI
SP
WP
Distance to the TC eye [km]
0 30 100 200 300 400 500

485 **Figure 3 Histograms of collocated RO profiles with: (a) Tropical Depressions, (b) Tropical Storms, (c) TCs category 1, (d) TCs category 2, (e) TCs category 3, (f) TCs category 4, (g) TCs category 5 for different ocean basins. Colours denote the distances between RO profile and the TC eye.**

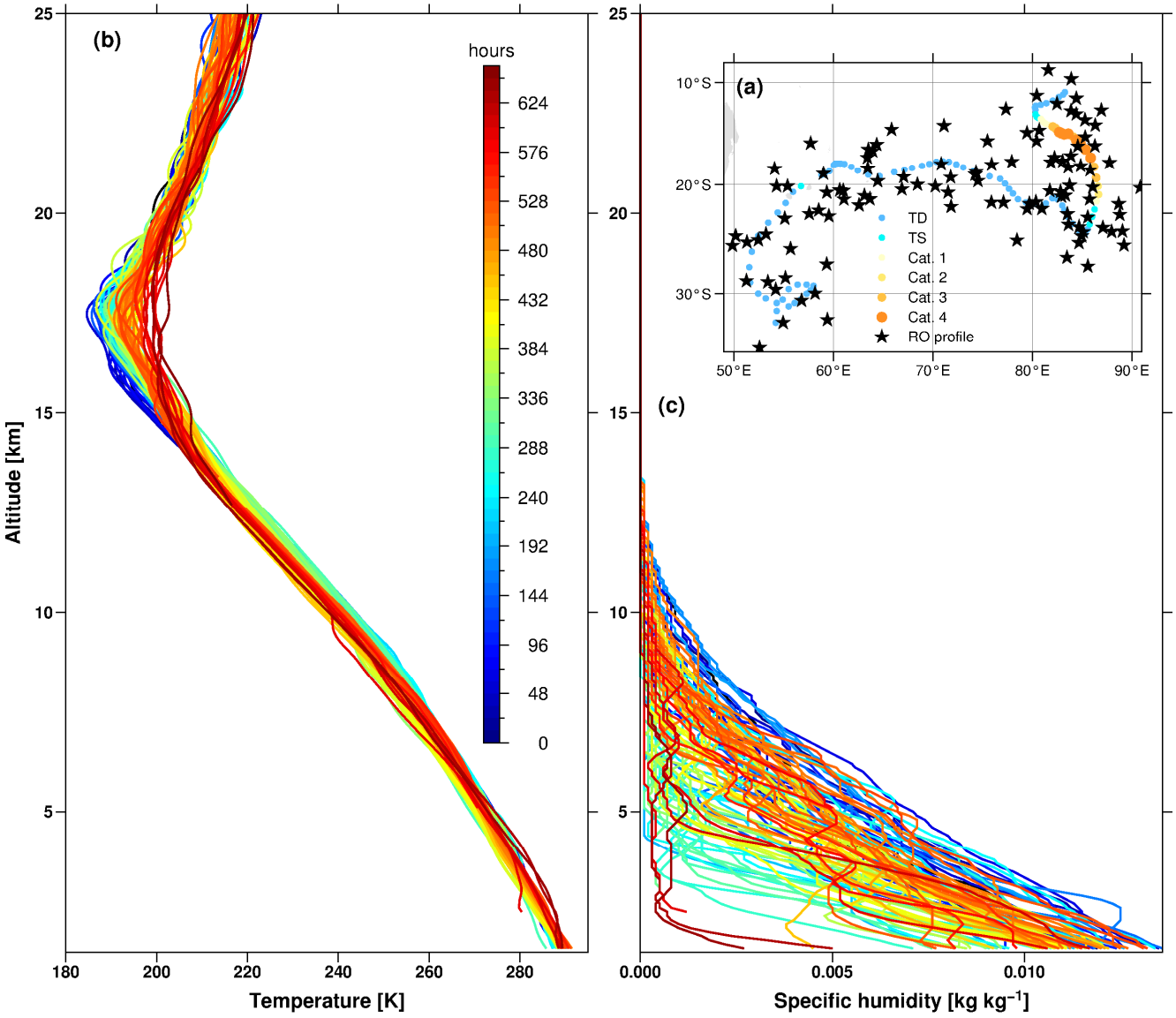

490 **Figure 4 Temporal evolution of the typhoon Hondo 2008. Hondo best track and co-located ROs (a). Temperature (b) and specific humidity (c) profiles from the surface to 25 km of altitude since the beginning to the end of the storm.**

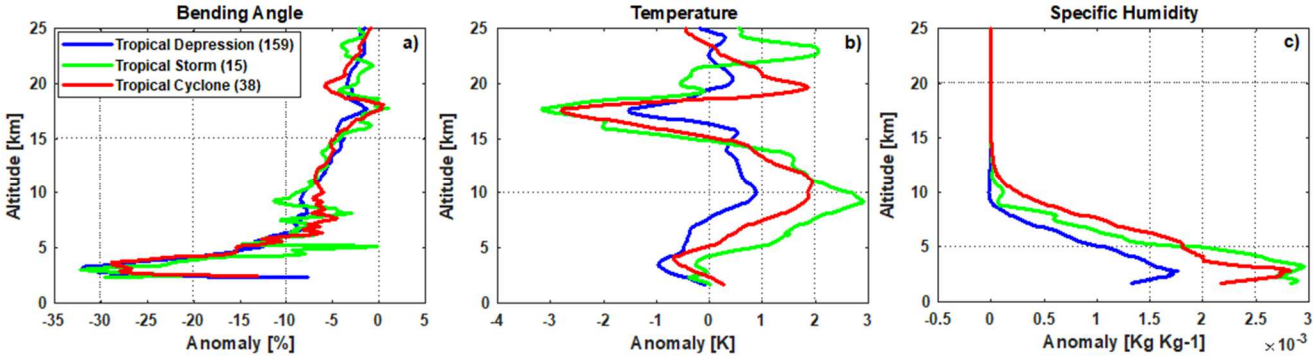

Figure 5 . Averaged bending angle anomaly (a), temperature anomaly (b) and specific humidity anomaly (c) profiles for the TD, TS and TC status of Hondo 2008.

495